Supporting Information

Bimetallic FeMn catalysts derived from metal organic frameworks efficient for photocatalytic removal of quinolones without oxidant

Xin Li,[a] Zhiyu Yang,[a] Di Hu,[a] Anqi Wang,[a] Yuwen Chen,[a] Yizhe Huang,[a] Man Zhang,[a]

Haoran Yuan[b] and Kai Yan*[a]

[a] *Guangdong Provincial Key Laboratory of Environmental Pollution Control and Remediation Technology, School of Environmental Science and Engineering, Sun Yat-sen University, 135 Xingang Xi Road, Guangzhou 510275, P. R. China*

[b] *Guangzhou Institute of Energy Conversion, Chinese Academy of Sciences, Guangzhou 510640, P. R. China*

[*] *Corresponding author E-mail addresses: yank9@mail.sysu.edu.cn (K. Yan)*

Contents

Materials

Ofloxacin (OFL, 98 %), ciprofloxacin (CIP, ≥98 %), enrofloxacin (ENR, 98 %), levofloxacin (LEV, >98 %) and norfloxacin (NOR, 98 %) were obtained from Aladdin (Shanghai, China). 1,3,5-benzenetricarboxylic acid (BTC, 98 %, Macklin), sodium hydroxide (NaOH, 97 %, Macklin), iron(III) nitrate nonahydrate ($Fe(NO_3)_3 \cdot 9H_2O$, 99.99 %, Macklin), Manganese(II) nitrate tetrahydrate ($Mn(NO_3)_2 \cdot 4H_2O$, 98 %, Aladdin), formic acid (HCOOH, ≥98 %, Aladdin), acetonitrile (C_2H_3N, ≥99.95 %, Fisher chemical), tert-butyl alcohol (TBA, 99.8 %, Alfa Aesar), EDTA disodium salt dihydrate (EDTA-2Na, 98 %, Macklin), p-benzoquinone (p-BQ, 99 %, Macklin), 2,2,6,6-tetramethylpiperidine-1-oxyl (TEMPO, 98 %, Macklin), furfuryl alcohol (FFA, 98 %, Macklin). All chemicals were at least analytical reagent and could be used directly without further purification. The water used in all experiments was ultra-pure deionized.

Characterization tools

The synthesized Fe-BTC, Fe_xMn_y (x: y = 2:1, 1:1, 1:2), pure Fe/Mn were characterized by X-ray diffraction (XRD, UltimalV) using Cu K*a* radiation (26 mA, 40 kV) at room temperature. The 2θ scanning angle range was from 5-90^o with a step of 5 ^{o}/min. Besides, Fourier transform-infrared spectroscopy (FT-IR, Nicolet iS50) was used to qualitatively analyze the functional groups in sample molecules. The morphology of the powders was collected by scanning electron microscopy (SEM, Sigma 500) with an acceleration voltage of 10 kV. The structural information was further collected by

transmission electron microscopy (TEM, FEI Tecnai G2 F20 electron microscope) accelerated at 200 kV with Electronic Differential System (EDS, OXFORD X-max 80T). The surface chemical states and valence band spectrum of FeMn were measured with an X-ray photoelectron spectroscopy/ESCA (XPS, ESCALAB 250) (Thermo Fisher Scientific) with Mono Al Kα source (energy 1486.6 eV). Ultraviolet visible diffuse reflectance (UVDF, UV-2600) was used to study the light absorption properties of FeMn samples. The quality change of Fe-BTC was monitored by TGA 5500, during the sample temperature program. The Brunauer-Emmett-Teller (BET) surface area and pore size distribution of FeMn were examined at 77 K by ASAP 2020 adsorption instrument, and samples were out-gassed under a vacuum at 120 °C for 8 h prior to the measurements. The concentration of total organic carbon (TOC) in the solution was analyzed by a TOC analyzer (Vario TOC select) after filtering through the membrane (0.22 μm size). The leaching of metal ions in the solution was examined by Inductively Coupled Plasma Optical Emission Spectrometer (ICP-OES, Perkin Elmer, Avio 500). Electron Paramagnetic resonance (EPR) spectra were recorded on a Bruker A300 spectrometer, and 5,5-dimethyl-1-pyrrolidine-N-oxide (DMPO) was applied as the spin-trapping agent.

Table S1 Parameters of specific surface areas and pore structures of the FeMn

Sample	Specific surface area ($m^2 g^{-1}$)	Total pore volume ($cm^3 g^{-1}$)	Average pore size (nm)
Fe_2Mn_1	73.6	0.26	14.0
Fe_1Mn_1	122.5	0.33	13.7
Fe_1Mn_2	100.4	0.33	12.6
Pure Fe	148.8	0.45	14.9

Table S2 Fe/Mn-based materials in the field of photocatalysis

Catalyst	Synthesis method	Contaminant	Reactivity	Mechanism	Refs.
MnO_2/Mn Fe_3O_4	Hydrothermal method	Rhodamine B 10 mg L^{-1}	[PMS] = 0.4 g L^{-1}, [catalyst] = 0.2 g L^{-1}, 98.0 % removal in 15 min	SO_4^{-}• and •OH	1
$Mn_{0.6}Zn_{0.4}$ Fe_2O_4	Citrate combustion method	BPA 0.1 mM	[PMS] = 0.5 mM, [catalyst] = 0.2 g L^{-1}, 95.8 % removal in 60 min	SO_4^{-}•, •OH and $^1O_2$	2
MnO_x-Fe_3O_4/bio char	One-step pyrolysis method	Ciprofloxacin 10 mg L^{-1}	[H_2O_2] = 68 mg L^{-1}, [catalyst] = 0.2 g L^{-1}, pH = 5.44, 92.8 % removal in 90 min	•OH and $O_2^{\bullet-}$	3
FeMn@N -C	Thermal decomposition	Clothianidin (CTD) 5 mg L^{-1}	[PMS] = 0.2 g L^{-1}, [catalyst] = 0.1 g L^{-1}, pH = 7, 100 % removal in 90 min	SO_4^{-}•, •OH and $^1O_2$	4
$MnFe_2O_4$ @C-NH_2	Hydrothermal synthesis	Ofloxacin 30 mg L^{-1}	[H_2O_2] = 29.4 mM, [catalyst] = 1.0 g L^{-1}, pH = 3.0, 63.8 % removal in 180 min	•OH	5

FeMn/bio char	One-step pyrolysis	Naphthalene 30 mg L^{-1}	$[H_2O_2]$ = 100 mM; [catalyst] = 1.0 g L^{-1}, pH = 5.6, 82.2 % removal in 148 min	•OH and $O_2^{\bullet-}$	6
FeMn@N CNTs	One-step pyrolysis	Acetamiprid 7.8 μM	[PMS] = 6.5 mM, [catalyst] = 0.1 g L^{-1}, pH = 7, 99.3 % removal in 90 min	SO_4^{-}•, •OH and $O_2^{\bullet-}$	7
Mn-Fe layered double hydroxide	Coprecipitation	Acid Orange 7 (AO7) 20 mg L^{-1}	[PMS] = 0.2 g L^{-1}, [catalyst] = 0.2 g L^{-1}, pH = 6.10, 97.6 % removal in 30 min	SO_4^{-}•, •OH	8
γ-Fe_2O_3-MIL-53 (Fe)-GO	The simple ethylenediamine pyrolysis and in situ hydrothermal method	Norfloxacin (NOR) 10 mg L^{-1}	[catalyst] = 0.2 g L^{-1}, 92.8 % in 90 min	h^+, ·OH, e^-	9
Fe_1Mn_1	Impregnation	CIP 20 mg L^{-1}	[Catalysts] = 0.1 g L^{-1}, pH = 7, T = 25 °C, 98.3 % removal in 30 min	•OH and $O_2^{\bullet-}$, h^+	this work

Table S3 The possible intermediates of CIP degradation in the Fe_1Mn_1/light system

Number	Formula	m/z	Proposed structure
CIP	$C_{17}H_{18}FN_3O_3$	331	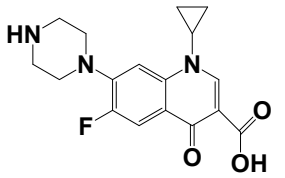
L1	$C_{17}H_{16}FN_3O_3$	329	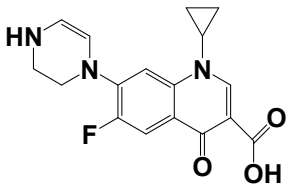
L2	$C_{17}H_{18}FN_3O_3$	347	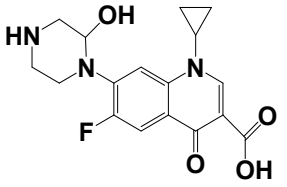
L3	$C_{17}H_{16}FN_3O_4$	345	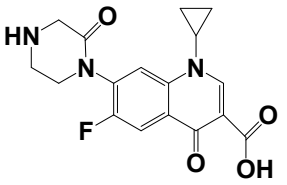
L4	$C_{17}H_{16}FN_3O_5$	361	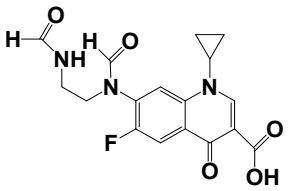
L5	$C_{17}H_{16}FN_3O_5$	361	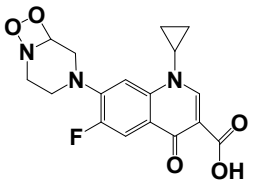
L6	$C_{13}H_{11}FN_2O_3$	262	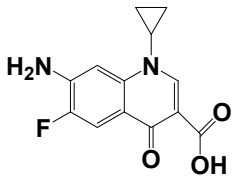
L7	$C_{10}H_9FN_2O_3$	224	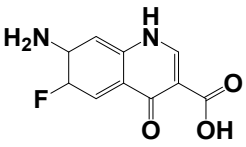

L8	$C_8H_5FN_2O_2$	180	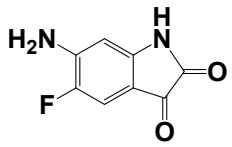
L9	$C_{17}H_{19}N_3O_4$	329	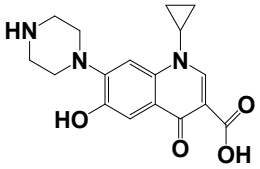
L10	$C_{17}H_{19}N_3O_5$	345	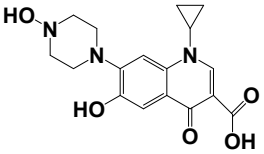
L11	$C_{17}H_{17}N_3O_6$	359	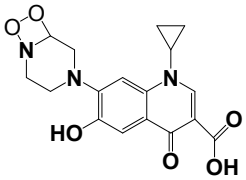
L12	$C_{13}H_{12}N_2O_4$	260	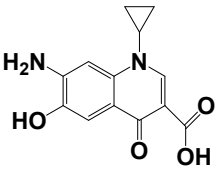
L13	$C_8H_8N_2O_4$	196	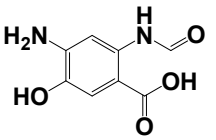
L14	$C_7H_6N_2O_3$	166	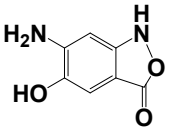
L15	$C_{15}H_{17}N_3O_3$	287	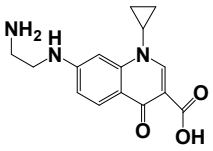
L16	$C_{13}H_{16}N_2O_3$	248	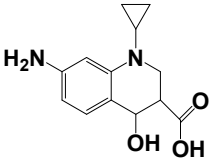
L17	$C_{10}H_{12}N_2O_3$	208	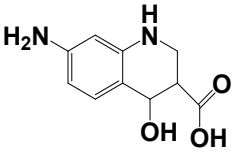

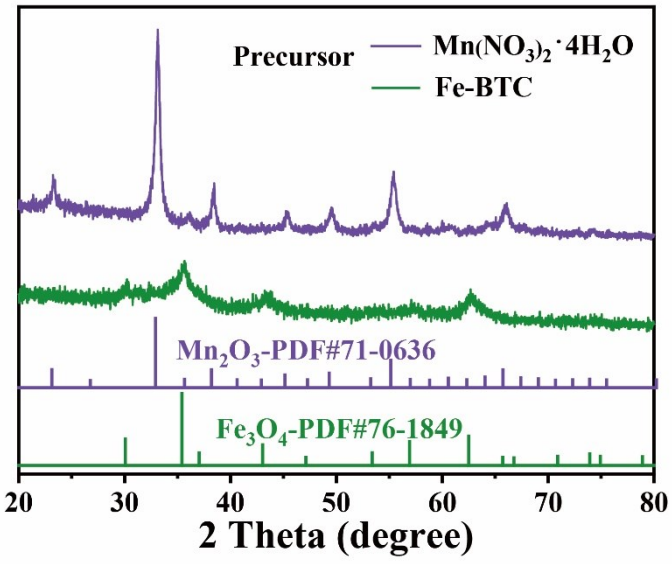

Fig. S1 XRD patterns of samples obtained with separate Fe-BTC or $Mn(NO_3)_2 \cdot 4H_2O$ precursors.

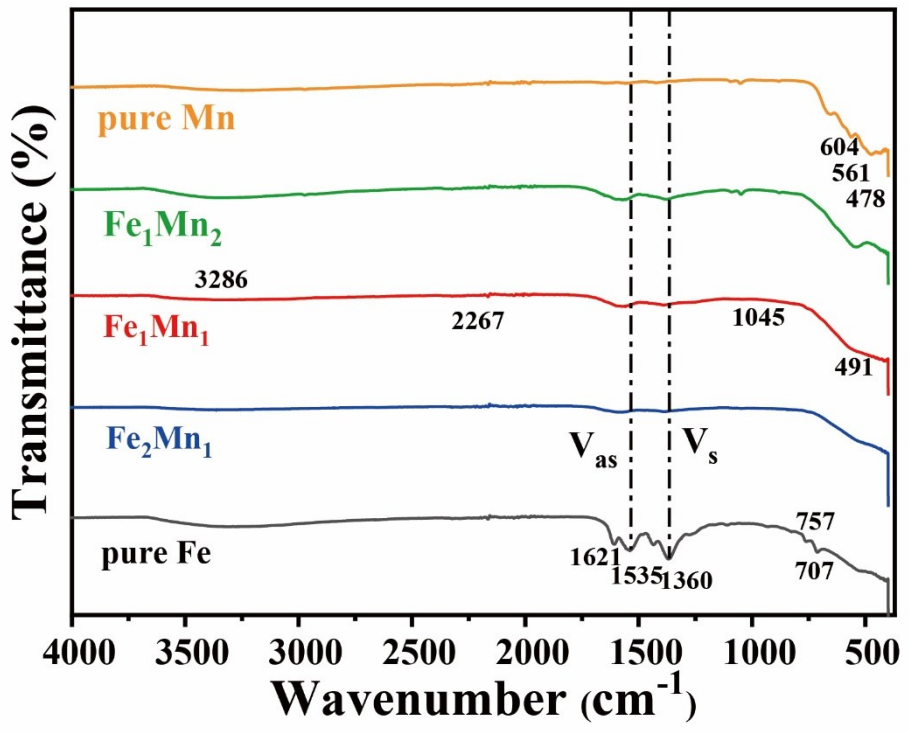

Fig. S2 FT-IR spectra of pure Fe/Mn, Fe_1Mn_2, Fe_1Mn_1, and Fe_2Mn_1 samples.

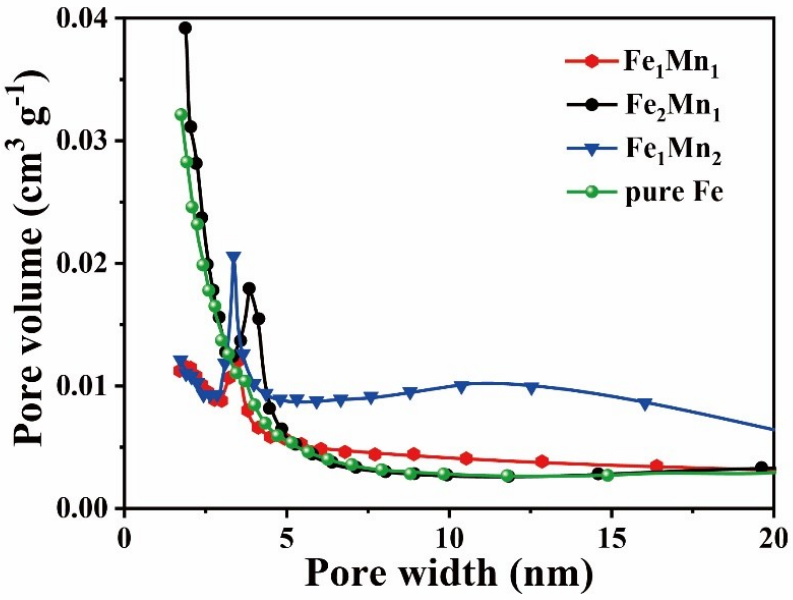

Fig. S3 Pore size distribution of synthetic materials FeMn catalysts.

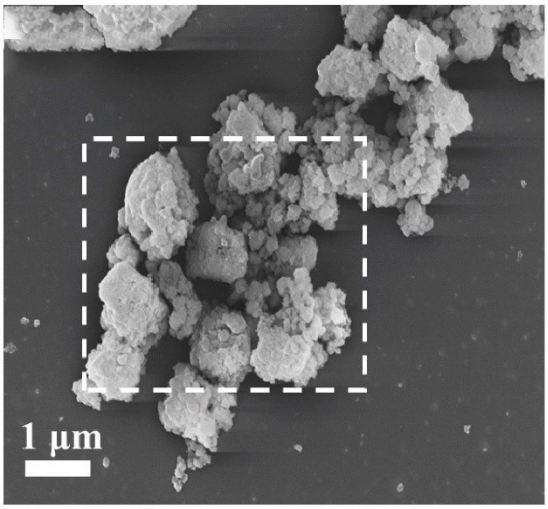

Fig. S4 SEM analysis of the fabricated Fe_1Mn_1 catalyst related to Fig. 3d.

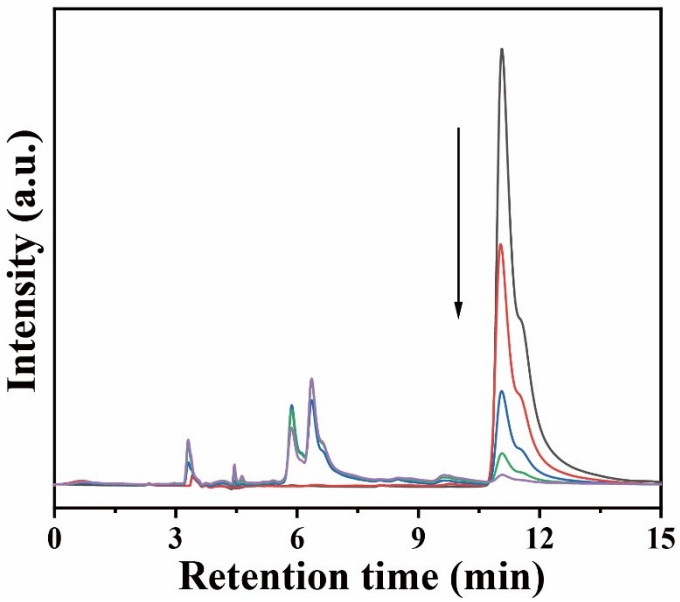

Fig. S5 HPLC chromatograms of CIP solution measured at different reaction time.

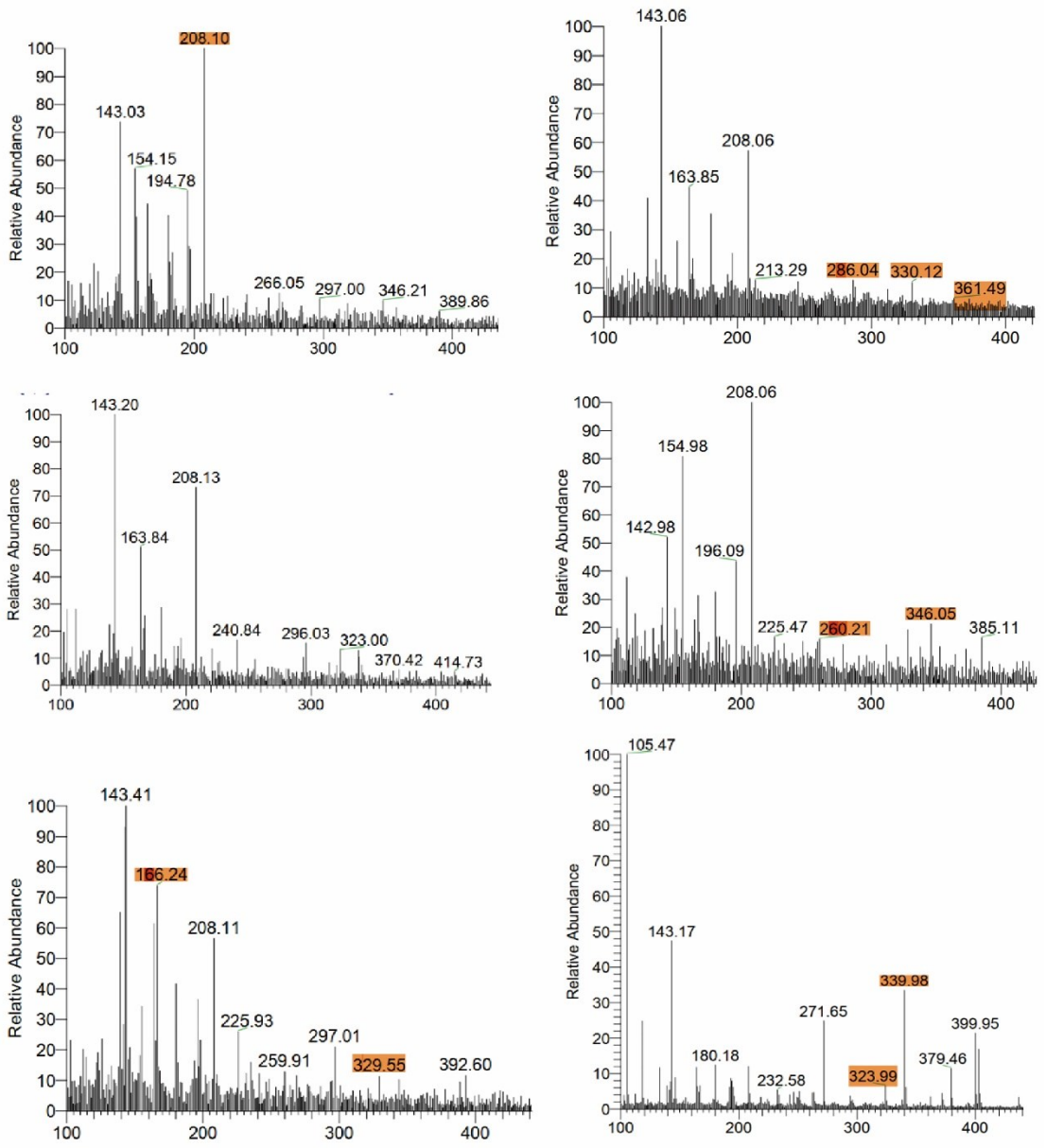

Fig. S6 Mass spectra and proposed structure of detected intermediate products.

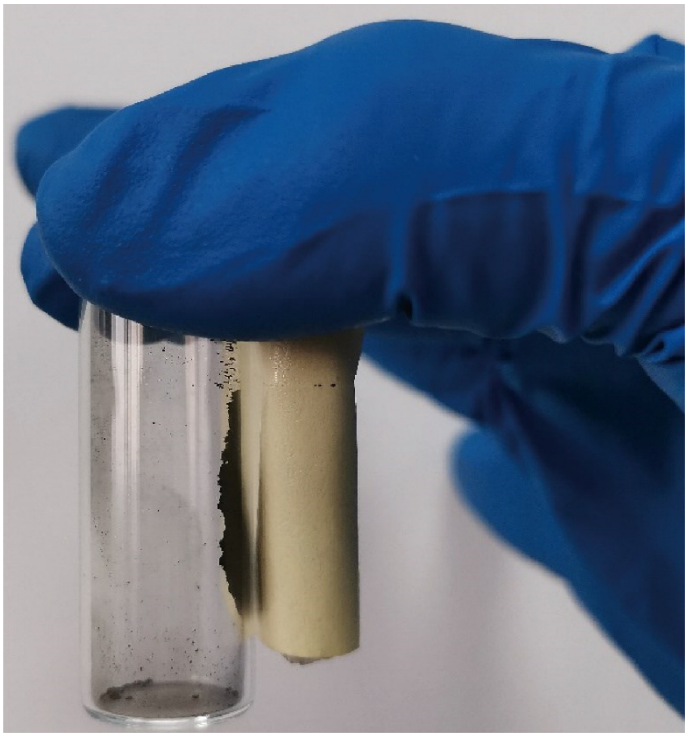

Fig. S7 Magnetic detection of Fe_1Mn_1 nanocomposite.

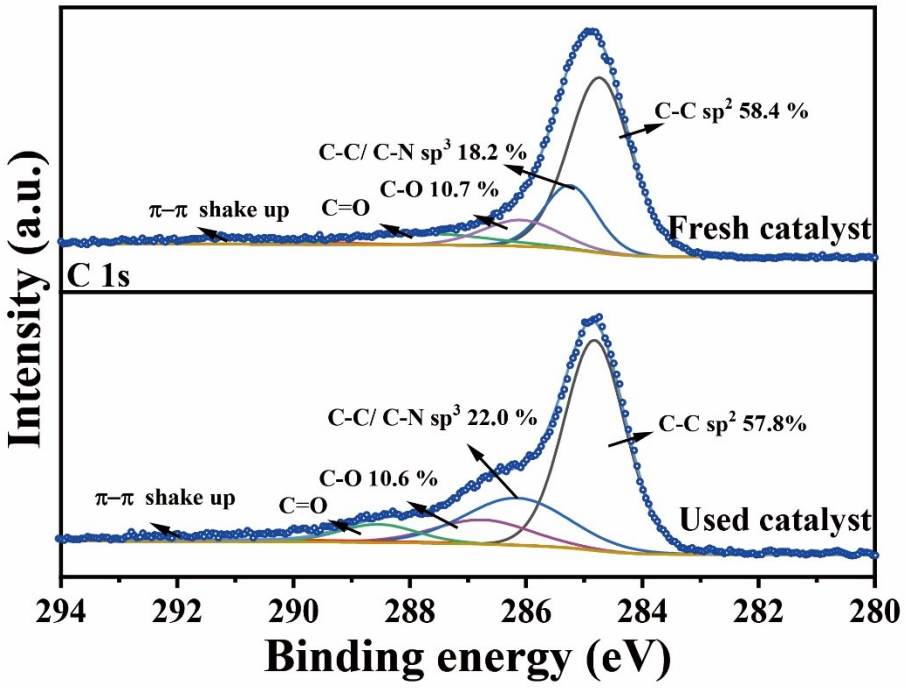

Fig. S8 XPS (C 1s) spectra of the Fe_1Mn_1 catalyst.

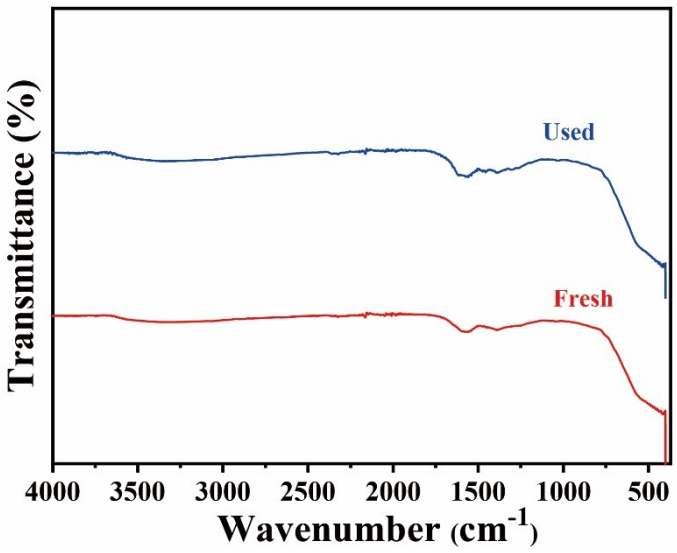

Fig. S9 FT-IR analysis of the fresh and reacted Fe_1Mn_1 catalyst.

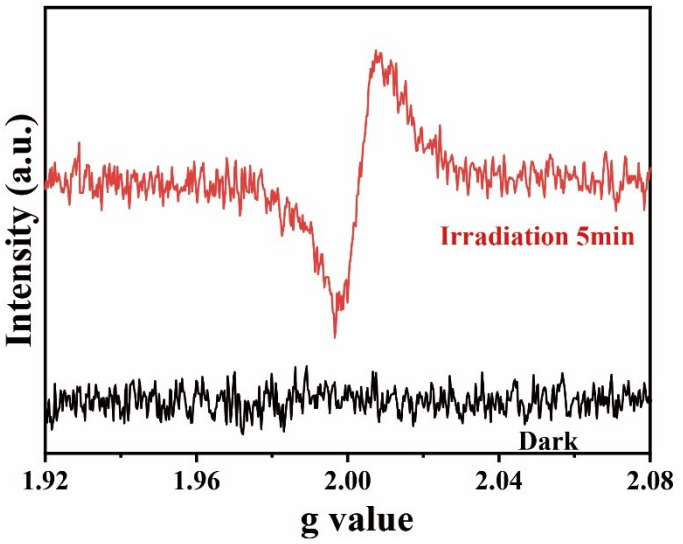

Fig. S10 g Value of the obtained catalysts before and after irradiation.

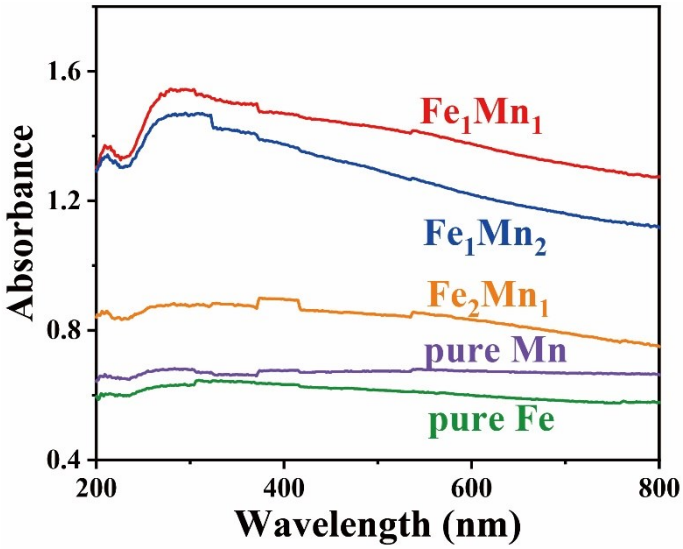

Fig. S11 UV-vis DRS spectra of FeMn samples.

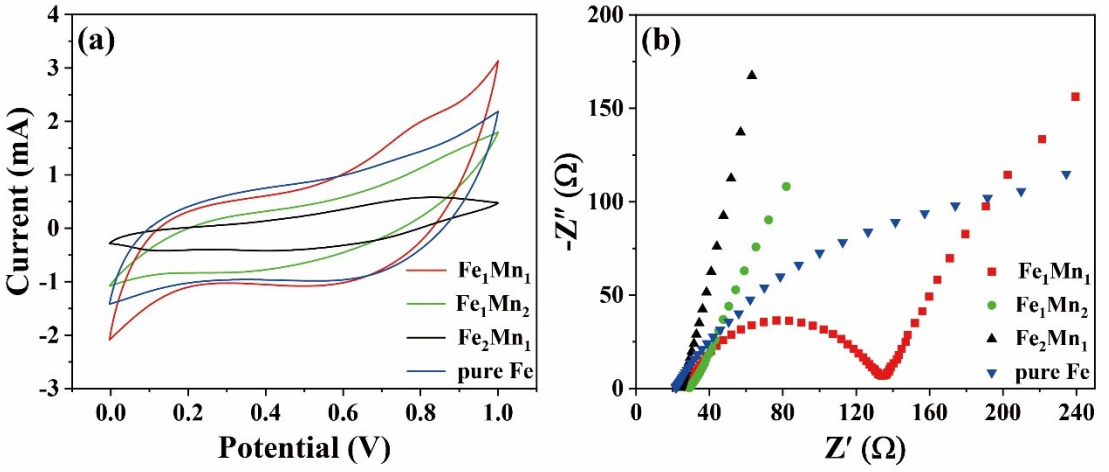

Fig. S12. (a) Cyclic voltammetry (CV) curves and (b) electrochemical impedance spectroscopy (EIS) spectra of Fe_1Mn_1, Fe_1Mn_2, Fe_2Mn_1 and pure Fe.

References

1. G. Chen, X. Zhang, Y. Gao, G. Zhu, Q. Cheng and X. Cheng, Novel magnetic $MnO_2/MnFe_2O_4$ nanocomposite as a heterogeneous catalyst for activation of peroxymonosulfate (PMS) toward oxidation of organic pollutants, *Sep. Purif. Technol.*, 2019, **213**, 456-464.
2. H. Lin, S. Li, B. Deng, W. Tan, R. Li, Y. Xu and H. Zhang, Degradation of bisphenol A by activating peroxymonosulfate with $Mn_{0.6}Zn_{0.4}Fe_2O_4$ fabricated from spent Zn-Mn alkaline batteries, *Chem. Eng. J.*, 2019, **364**, 541-551.
3. L. Li, S. Liu, M. Cheng, C. Lai, G. Zeng, L. Qin, X. Liu, B. Li, W. Zhang, Y. Yi, M. Zhang, Y. Fu, M. Li and M. Long, Improving the Fenton-like catalytic performance of MnO_x-Fe_3O_4/biochar using reducing agents: A comparative study, *J. Hazard. Mater.*, 2021, **406**, 124333.
4. P. Duan, Y. Qi, S. Feng, X. Peng, W. Wang, Y. Yue, Y. Shang, Y. Li, B. Gao and X. Xu, Enhanced degradation of clothianidin in peroxymonosulfate/catalyst system via core-shell FeMn @ N-C and phosphate surrounding, *Appl. Catal. B: Environ.*, 2020, **267**, 118717.
5. H. Qin, H. Cheng, H. Li and Y. Wang, Degradation of ofloxacin, amoxicillin and tetracycline antibiotics using magnetic core-shell $MnFe_2O_4$@C-NH_2 as a heterogeneous Fenton catalyst, *Chem. Eng. J.*, 2020, **396**, 125304.
6. L. Li, C. Lai, F. Huang, M. Cheng, G. Zeng, D. Huang, B. Li, S. Liu, M. Zhang, L. Qin, M. Li, J. He, Y. Zhang and L. Chen, Degradation of naphthalene with magnetic bio-char activate hydrogen peroxide: Synergism of biochar and Fe-Mn binary oxides, *Water Res.*, 2019, **160**, 238-248.
7. P. Duan, T. Ma, Y. Yue, Y. Li, X. Zhang, Y. Shang, B. Gao, Q. Zhang, Q. Yue and X. Xu, Fe/Mn nanoparticles encapsulated in nitrogen-doped carbon nanotubes as a peroxymonosulfate activator for acetamiprid degradation, *Environ. Sci.: Nano*, 2019, **6**, 1799-1811.
8. L. Hou, X. Li, Q. Yang, F. Chen, S. Wang, Y. Ma, Y. Wu, X. Zhu, X. Huang and D. Wang, Heterogeneous activation of peroxymonosulfate using Mn-Fe layered double hydroxide: Performance and mechanism for organic pollutant degradation, *Sci. Total Environ.*, 2019, **663**, 453-464.
9. Q. Wu, Y. Liu, H. Jing, H. Yu, Y. Lu, M. Huo and H. Huo, Peculiar synergetic effect of γ-Fe_2O_3 nanoparticles and graphene oxide on MIL-53 (Fe) for boosting photocatalysis, *Chem. Eng. J.*, 2020, **390**, 124615.